Inter-Operator Reliability of an Onsite Machine Learning-Based Prototype to Estimate Ct Angiography-Derived Fractional Flow Reserve

Yushui Han
Houston Methodist Research Institute https://orcid.org/0000-0002-8357-9729
Ahmed Ibrahim Ahmed
Houston Methodist Research Institute
Chris Schwemmer
Siemens Healthcare GmbH
Myra Cocker
Siemens Medical Solutions USA Inc: Siemens Healthcare USA
Talal S Alnabelsi
Houston Methodist Research Institute
Jean michel Saad
Houston Methodist Research Institute
Juan C Ramirez Giraldo
Siemens Medical Solutions USA Inc: Siemens Healthcare USA
Mouaz H Al-Mallah (mal-mallah@houstonmethodist.org)
Houston Methodist Research Institute https://orcid.org/0000-0003-2348-0484

Research Article

Keywords: Computed Tomography, Fractional Flow Reserve, Inter-operator Reliability, Machine Learning, Computed tomography angiography

Posted Date: August 13th, 2021

DOI: https://doi.org/10.21203/rs.3.rs-741234/v1

Abstract

Background: Advances in computed tomography (CT) and machine learning have enabled on-site non-invasive assessment of fractional flow reserve (FFR_{CT}).

Purpose: To assess the inter-operator variability of Coronary CT Angiography–derived FFR_{CT} using a machine learning based post-processing prototype.

Materials and Methods: We included 60 symptomatic patients who underwent coronary CT angiography. FFR_{CT} was calculated by 2 independent operators after training using a machine learning based on-site prototype. FFR_{CT} was measured 1 cm distal to the coronary plaque or in the middle of the segments if no coronary lesions were present. Intraclass correlation coefficient (ICC) and Bland-Altman analysis were used to evaluate inter-operator variability effect in FFR_{CT} estimates. Sensitivity analysis was done by cardiac risk factors, degree of stenosis and image quality.

Results: A total of 535 coronary segments in 60 patients were assessed**.** The overall ICC was 0.986 per patient (95% CI: 0.977 - 0.992) and 0.972 per segment (95% CI: 0.967 - 0.977). The absolute mean difference in FFR_{CT} estimates was 0.012 per patient (95% CI for limits of agreement: -0.035 - 0.039) and 0.02 per segment (95% CI for limits of agreement: -0.077 - 0.080). Tight limits of agreement were seen on Bland-Altman analysis. Distal segments had greater variability compared to proximal/mid segments (absolute mean difference 0.011 vs 0.025, $p<0.001$). Results were similar on sensitivity analysis.

Conclusion: A high degree of inter-operator reproducibility can be achieved by onsite machine learning based FFR_{CT} assessment. Future research is required to evaluate the physiological relevance and prognostic value of FFR_{CT}.

Introduction

The role of fractional flow reserve (FFR) assessment in the evaluation and management of patients with coronary artery disease was firmly established by the FAME (Fractional Flow Reserve versus Angiography for Guiding Percutaneous Coronary Intervention) trial, which demonstrated that an FFR guided percutaneous coronary intervention (PCI) strategy was superior at reducing the rates of death, myocardial ischemia and repeat revascularization at 1 year[1]. However, the need for an invasive angiography and its attendant risks limited routine use in clinical practice.

Advances in computational fluid dynamics (CFD), a noninvasive image post-processing technique, enabled the determination of physiologic significance of coronary artery stenosis by using data acquired from standard, routine diagnostic coronary cardiac tomography angiography (CCTA) studies. Machine learning based flow assessment is the latest development using an artificial intelligence algorithm to compute the functional severity of a lesion[2–4]. Machine learning (ML) based FFR_{CT} determination enables a rapid on-site determination by the reading physician, providing timely point-of-care information without the potential risks to patient privacy arising from off-site data transfer.

ML based FFR_{CT} requires semi-automatic determination of centerline, lumen contour and stenosis area, all of which potentially contributing to variability. Although several studies have shown similar sensitivity and specificity to computational fluid dynamics-based determination,[5] research is lacking on reproducibility of this operator dependent technology. The purpose of this study is to measure the inter-operator reliability and determine the reproducibility of Coronary CT Angiography–derived Fractional Flow Reserve (FFR_{CT}) values using a post-processing prototype based on machine learning algorithm.

Method

Patient population

The study population was defined as patients who underwent both clinically indicated CCTA and single photon emission computed tomography (SPECT) myocardial perfusion imaging (MPI) for suspected coronary artery disease between January 1, 2016 through June 22, 2020 (n = 965). Next, patients with prior percutaneous coronary intervention (PCI), coronary artery bypass grafts (CABG) and left ventricular assist devices (LVAD) were excluded (n = 258, 93 and 2 respectively). Moreover, patients with congenital abnormalities of the coronary tree (n = 12) and those with severe valvular abnormalities (n = 30) were also excluded. Lastly, patients who could not be processed by the FFR_{CT} prototype were excluded due to excessive calcification or poor image quality (n = 74). A cohort of 496 patients was obtained following the application of the above exclusions.

60 patients were randomly selected using simple random sampling without replacement. Sampling was stratified by categories of stenosis using Society of Cardiovascular Computed Tomography Coronary Artery Disease Reporting & Data System (CAD-RADS). Approval from the Institutional Review Board was obtained prior to the start of the study and informed consent was waived due to the retrospective nature of the study.

Assessment of Covariates

Information on sociodemographic variables (age and gender), medical history, comorbidities (hypertension, diabetes, dyslipidemia), smoking history and medication use was obtained from chart review of all patient profiles in electronic medical records within 30 days of imaging.

CCTA

CCTA scans were obtained using 3rd generation SOMTAM FORCE Scanner (Siemens, Forchheim, Germany) or Phillips 64 slice CT (Philips Healthcare, Amsterdam, Netherlands). Image acquisition was performed in accordance with the Society of Cardiovascular Computed Tomography (SCCT) guidelines[6]. Intravenous metoprolol was administered for patients with a heart rate > = 65 beats/min and sublingual nitroglycerin 0.4 mg was administered immediately before image acquisition. During image acquisition, 60-100cc of contrast was injected, followed by saline flush. Axial scans were obtained with prospective electrocardiographic gating. Image acquisition was prescribed to include the coronary arteries, left ventricle and proximal ascending aorta.

Images were assessed with a 3-dimensional workstation using one of several post-processing methods including axial, multiplanar reformat, maximum intensity projection and cross-sectional analysis. The quality of scans was determined by expert opinion and qualitatively graded as fair, good and excellent. Type and location of lesion were visually evaluated using an 18-segment model according to SCCT guidelines.[6] In each segment, atherosclerosis was defined as tissue structures > $1mm^2$ within the coronary artery lumen or adjacent to the lumen that could be discriminated from pericardial tissue, epicardial fat or vessel lumen itself.

Percent coronary stenosis was quantified based on a comparison of the luminal diameter of the segment exhibiting obstruction to the luminal diameter of the most normal-appearing site and classified as none (0%), mild (1–49%), moderate (50–69%), or severe (> = 70%) based on degree of narrowing of the luminal diameter Anatomically obstructive CAD by CCTA was defined as > = 50% in the left main artery and > = 70% stenosis severity in proximal, mid and distal branches of the left anterior descending, left circumflex and right coronary artery without including side branches. Findings were reported using Society of Cardiology Computed Tomography Coronary Artery Disease Reporting & Data System (CAD-RADS).[7]

Segment involvement score (SIS) was used to quantify burden of disease using CCTA. Using an 18-segment coronary artery model, each segment was individually scored as 0 or 1 based on the presence of plaque irrespective of the degree of stenosis. The sum of all involved segments was calculated for each patient. A Hounsfield unit threshold of > = 130 was used to classify plaques composition as Calcified (C SIS), Mixed (M SIS), Calcified or Mixed (C/M SIS) and Non-Calcified plaque (NC SIS).

FFR_{CT}

FFR_{CT} was determined using a machine learning based prototype for computation of fractional flow reserve (cFFR 3.2, Siemens Healthcare GmbH, Forchheim, Germany).

CCTA accusation phase was chosen based on heart rate and absence of motion. The best diastolic phase was selected for heart rate < 65 bpm, while the best systolic phase was used when heart rate > = 65 bpm. The coronary tree was isolated semi-automatically to generate a 3-dimentional model. The extent of manual adjustment was proportional to severity and extent of calcification, with most cases requiring limited adjustment of centerline and contour.

The algorithm generated a value for every point of the coronary artery tree using the ratio of the average aortic and local pressure over a cardiac cycle. A 3-dimensional color-coded mesh of the coronary artery tree was created in combination with functional information at each segment of interest. FFR_{CT} was determined at the mid-point of a vessel segment for normal vessels and 1 cm distal to stenosis when one was present based on prior work showing higher prognostic role of measurements distal to stenosis [8]. Determination was made for the left main (LM) and proximal, mid and distal segments of the left anterior descending (LAD), left circumflex (LCX) and right coronary artery (RCA) without including side branches. Vessel segments that could not be isolated by the prototype were coded as missing. FFR_{CT} of < 0.8 in the LM or any proximal, mid or distal segment was considered as the threshold for significant ischemia based on prior literature. [9–12]

Image processing was done by two investigators blinded to results from other tests. Both had backgrounds in the health sciences (one with a medical degree and another with a master's in biomedical engineering) but no prior experience with CCTA or FFR_{CT} processing. Training was organized by the vendor on the steps of image processing. Investigators subsequently processed and received feedback on the first 20 set of patients. Experts from the vendor were consulted on difficult cases throughout the data collection phase. Each investigator did two rounds of processing for each patient. During the second round, processing was started from the beginning without using persistent data from the prior round.

Supplemental Fig. 1 demonstrated the prototype interface and FFR_{CT} results of the same patient case processed by 2 operators.

Statistical Analysis

Analysis was done on a per-patient and per-segment level. For per-patient analysis, the mean FFR_{CT} from all isolated segments of the coronary artery were used. Per-segment analysis was stratified by each segment and as a comparison between proximal (LM and proximal branches of LAD, LCX and RCA) vs distal segments. Both inter and intra-investigator agreement was assessed. The average of two rounds of processing was used for inter-investigator analysis, and percent reclassification was determined using an FFR_{CT} threshold of < 0.8.

The mean difference with 95% limits of agreement and intra-class correlation coefficient (ICC) using two-way mixed effect model were used to assess for agreement. Thresholds for agreement were classified based on prior literature (< 0.2, poor; 0.2 to 0.4, fair; 0.4 to 0.6-moderate; 0.6 to 0.8, good; 0.8 to 1.0, very good)[13]. Furthermore, Bland-Altman analysis was used to evaluate for variability. All analyses were done using Stata 16.0 (StataCorp, College Station, Texas)

Results

Sociodemographic

Sixty (60) patients were included in this study. Baseline characteristics are listed in Table 1. The mean age was 63.5 + 11.7 years and 45% were women. The majority had cardiovascular comorbidities: 78% hypertension, 68%% diabetes and 87% dyslipidemia. Most patients (52%) were symptomatic with chest pain or shortness of breath and a majority were on some form of medication (83% aspirin/clopidogrel, 83% statin, 65% angiotensin converting enzyme inhibitor/angiotensin receptor blocker.)

Table 1
Baseline characteristics of patients

	Total
	N = 60
Sociodemographics	
Age - Mean(SD)	*63.50 (11.65)*
Gender - N(%)	
Female	*27 (45%)*
Comorbidities - *N(%)*	
Hypertension	*47 (78%)*
Diabetes	*41 (68%)*
Dyslipidemia	*52 (87%)*
Symptoms - *N(%)*	
Chest Pain or Shortness of Breath	*31 (52%)*
Medication - *N(%)*	
Aspirin/Clopidogrel	*50 (83%)*
Statin	*50 (83%)*
ACE/ARB	*39 (65%)*
Beta Blockers	*46 (77%)*
Calcium Channel Blockers	*25 (42%)*
Study Quality - *N(%)*	
Excellent	*20 (33%)*
Good	*30 (50%)*
Fair	*10 (17%)*
CCTA - *N(%)*	
CCTA CAD-RAD	
CAD-RAD 0	*13 (22%)*
CAD-RAD 1/2	*24 (40%)*
CAD-RAD 3	*11 (18%)*
CAD-RAD 4A	*7 (12%)*
CAD-RAD 4B	*5 (8%)*
CCTA obstructive stenosis	*9 (15%)*
CCTA Multi-Vessel Disease	*5 (8%)*
Plaque Burden - *Mean(SD)*	
Total Plaque Segment Involvement Score	*4.60 (4.09)*
Calcified Plaque Segment Involvement Score	*1.95 (2.91)*
Mixed Plaque Segment Involvement Score	*2.05 (3.06)*
Non-Calcified Plaque Segment Involvement Score	*0.60 (1.34)*
FFRct - *N(%)*	
FFRct < 0.80 on any proximal/mid/distal segment	*28 (47%)*
Left Main FFRct < 0.8	*1 (2%)*
Major LAD segment FFRct < 0.80	*18 (30%)*
Major LCx segment FFRct < 0.80	*14 (23%)*

	Total
Major RCA segment FFRct < 0.80	*14 (24%)*

CCTA

More than half (83%) of CCTA's image quality was graded as excellent or good by reading physicians. Most patients had CAD-RAD scores < = 2 (62%) and the mean(SD) segment involvement score(SIS) was 4.6(+/-4.09.) Obstructive stenosis was present in 9 (15%) patients and 5 (8%) had multivessel disease. Nearly half (47%) of patients had functional stenosis (FFR_{CT}<0.8), and the LAD was the most affected vessel.

Intra-investigator agreement

Supplemental Table 1 summarizes measures of intra-investigator agreement. There was a high degree agreement between the two measurements taken by the same investigator. Per-patient and per-segment ICC's were > 0.95 for both investigators, with higher ICC's in proximal vs distal segments. Absolute differences showed similar trends, with tight limits of agreement.

Inter-investigator agreement

Table 2 summarizes measures of inter-investigator agreement. Per-patient and per-segment ICC was 0.986 per patient (95% CI: 0.977–0.992) and 0.972 per segment (95% CI: 0.967–0.977). The absolute mean difference in estimates was 0.012 per patient (the 95% CI for limits of agreement: -0.035–0.039) and 0.02 per segment (the 95% CI for limits of agreement: -0.077–0.080). Distal segments had greater variability compared to proximal/mid segments (ICC 0.97 vs 0.962 and absolute mean difference 0.011 vs 0.025 for proximal vs distal segments). Using a threshold of FFR_{CT}<0.8, per-patient discordance was seen in 3.3%(n = 2) patients.

Table 2. Inter-investigator agreement

	ICC		Difference	
Segment		**95% CI**	**Absolute Mean Difference**	**Bland Altman Limits of Agreement**
Average				
Per Patient	0.986	0.977 - 0.992	0.012	-0.035 - 0.039
Per-Segment	0.972	0.967 - 0.977	0.02	-0.077 - 0.080
Per-Segment (Proximal)	0.970	0.962 - 0.977	0.011	-0.050 - 0.046
Per-Segment (Distal)	0.962	0.953 - 0.969	0.025	-0.087 - 0.089
Per-Segment				
Left Main	0.972	0.953 - 0.983	0.005	-0.025 - 0.021
LAD				
Proximal	0.949	0.915 - 0.969	0.014	-0.046 - 0.049
Mid	0.976	0.960 - 0.986	0.024	-0.067 - 0.068
Distal	0.964	0.940 - 0.978	0.032	-0.098 - 0.107
LCX				
Proxmial	0.973	0.955 - 0.984	0.015	-0.079 - 0.069
Mid	0.975	0.958 - 0.985	0.027	-0.077 - 0.075
RCA				
Proximal	0.974	0.957 - 0.984	0.009	-0.035 - 0.031
Mid	0.979	0.965 - 0.988	0.019	-0.065 - 0.074
Distal	0.958	0.930 - 0.975	0.038	-0.136 - 0.154

Figures 1 & 2 show Bland-Altman graphs per-patient and per-segment. Tight limits of agreement were seen on all analysis, with relatively wider margins on distal vs proximal segments.

Tables 3 and 4 summarize measures of agreement by CAD-RAD and quality of CCTA scans. Absolute mean difference increased with higher CAD-RAD scores and lower quality. Results were more variable with ICC. Table 5 summarizes measures of agreement comparing patients with cardiovascular risk factors. Absolute mean differences were lower and ICC was higher amongst those without vs with risk factors.

Table 3. Inter-investigator agreement by CAD-RAD

	CAD-RAD 0				CAD-RAD 1/2				CAD-RAD >2			
	ICC		Difference		ICC		Difference		ICC		Difference	
		95% CI	Absolute Mean Difference	Bland Altman Limits of Agreement		95% CI	Absolute Mean Difference	Bland Altman Limits of Agreement		95% CI	Absolute Mean Difference	Bland Altman Limits of Agreement
Average												
Per Patient	0.841	0.558 - 0.949	0.008	-0.038 - 0.034	0.975	0.944 - 0.989	0.011	-0.028 - 0.038	0.988	0.972 - 0.995	0.016	-0.040 - 0.041
Per-Segment	0.729	0.631 - 0.804	0.014	-0.085 - 0.082	0.960	0.949 - 0.970	0.018	-0.058 - 0.068	0.981	0.974 - 0.985	0.027	-0.090 - 0.089
Per-Segment (Proximal)	0.801	0.678 - 0.881	0.005	-0.016 - 0.017	0.976	0.965 - 0.984	0.008	-0.026 - 0.032	0.969	0.954 - 0.979	0.017	-0.077 - 0.060
Per-Segment (Distal)	0.741	0.640 - 0.826	0.013	-0.042 - 0.036	0.947	0.928 - 0.962	0.024	-0.063 - 0.083	0.968	0.956 - 0.977	0.033	-0.121 - 0.110

Table 4. Inter-investigator agreement by image quality

	Excellent				Good				Fair			
	ICC		Difference		ICC		Difference		ICC		Difference	
		95% CI	Absolute Mean Difference	Bland Altman Limits of Agreement		95% CI	Absolute Mean Difference	Bland Altman Limits of Agreement		95% CI	Absolute Mean Difference	Bland Altman Limits of Agreement
Average												
Per Patient	0.985	0.962 - 0.994	0.007	-0.016 - 0.021	0.980	0.959 - 0.991	0.014	-0.039 - 0.047	0.982	0.930 - 0.996	0.018	-0.047 - 0.037
Per-Segment	0.947	0.930 - 0.960	0.014	-0.052 - 0.057	0.974	0.967 - 0.979	0.02	-0.080 - 0.086	0.966	0.948 - 0.977	0.034	-0.106 - 0.096
Per-Segment (Proximal)	0.764	0.654 - 0.842	0.006	-0.022 - 0.022	0.984	0.978 - 0.989	0.01	-0.038 - 0.039	0.940	0.889 - 0.968	0.022	-0.103 - 0.076
Per-Segment (Distal)	0.918	0.806 - 0.967	0.012	-0.028 - 0.035	0.977	0.951 - 0.989	0.026	-0.074 - 0.080	0.952	0.820 - 0.988	0.049	-0.120 - 0.112

Table 5. Inter-investigator agreement by cardiovascular risk factors

	Hypertensives				Normotensives			
	ICC		Difference		ICC		Difference	
		95% CI	Absolute Mean Difference	Bland Altman Limits of Agreement		95% CI	Absolute Mean Difference	Bland Altman Limits of Agreement
Per Patient	0.985	0.974 - 0.992	0.013	-0.036 - 0.043	0.991	0.971 - 0.997	0.008	-0.025 - 0.020
Per-Segment	0.976	0.971 - 0.980	0.021	-0.076 - 0.081	0.935	0.908 - 0.954	0.019	-0.082 - 0.077
Per-Segment (Proximal)	0.981	0.974 - 0.985	0.01	-0.042 - 0.039	0.902	0.835 - 0.942	0.012	-0.071 - 0.066
Per-Segment (Distal)	0.965	0.956 - 0.972	0.027	-0.094 - 0.098	0.928	0.893 - 0.955	0.017	-0.053 - 0.047
	Diabetics				Non-diabetics			
	ICC		Difference		ICC		Difference	
		95% CI	Absolute Mean Difference	Bland Altman Limits of Agreement		95% CI	Absolute Mean Difference	Bland Altman Limits of Agreement
Per Patient	0.985	0.971 - 0.992	0.013	-0.036 - 0.042	0.990	0.974 - 0.996	0.01	-0.032 - 0.030
Per-Segment	0.968	0.961 - 0.974	0.022	-0.082 - 0.087	0.982	0.976 - 0.987	0.017	-0.065 - 0.063
Per-Segment (Proximal)	0.970	0.960 - 0.978	0.011	-0.052 - 0.052	0.973	0.958 - 0.983	0.009	-0.042 - 0.030
Per-Segment (Distal)	0.958	0.946 - 0.967	0.024	-0.069 - 0.079	0.969	0.956 - 0.979	0.028	-0.118 - 0.104
	Dyslipidemics				Non-dyslipidemics			
	ICC		Difference		ICC		Difference	
		95% CI	Absolute Mean Difference	Bland Altman Limits of Agreement		95% CI	Absolute Mean Difference	Bland Altman Limits of Agreement
Per Patient	0.986	0.975 - 0.992	0.013	-0.037 - 0.041	0.959	0.809 - 0.992	0.006	-0.017 - 0.015
Per-Segment	0.974	0.968 - 0.978	0.022	-0.079 - 0.083	0.840	0.755 - 0.898	0.012	-0.061 - 0.059
Per-Segment (Proximal)	0.970	0.961 - 0.977	0.012	-0.054 - 0.049	0.964	0.928 - 0.982	0.004	-0.014 - 0.018
Per-Segment (Distal)	0.963	0.954 - 0.970	0.027	-0.091 - 0.095	0.787	0.668 - 0.880	0.013	-0.041 - 0.035

Discussion

Using a randomly selected sample from a real-world single-center cohort of patients, we demonstrated that machine learning based ML-FFR_{CT} determination has good reproducibility and reliability.

Non-invasive determination of FFR has the potential to further enhance the gate-keeper role of CT angiography in patients evaluated for coronary artery disease by providing a functional compliment to anatomic assessment[14]. Machine learning based FFR determination takes this one step further by offering several distinct advantages all the while maintaining comparative test characteristics to the current computational fluid dynamics-based approach[4,15].Specifically the advantages of a switch from off-site to on-site ML-based FFR determination may translate into reductions in test turn-around time (currently as high as 24 hours), rejection rate (~ 15%),[16–18] and cost combined with increased patient data protection by eliminating the need for data exporting and related infrastructural and logistical considerations .

Of the few studies that have looked at reproducibility of non-invasive FFR measurement, most have been on computational fluid dynamics-based methods. For example, a study with repeated off-site non-invasive FFR_{CT} measurement (CFD-based method) on 25 patients showed good reproducibility. The study also went on report no significant difference when comparing FFR_{CT} with FFR obtained from an invasive gold standard.[19] However, few studies tackled potential operator dependence similar to the aim of our study. These studies featuring both on-site and off-site approaches have reported a high degree of inter-operator correlation which was consistent among operators of different expertise and training.[20,21] Moreover, the previously cited study also emphasized decreased variabilities in operators receiving face-to-face training [20]. As such in-person training may counter a potential source of variability which has been the incorrect determination of centerline[20,22].

A case can be made to the generalizability of our findings to those presenting to a tertiary care cardiology practice as our study used a representative sample from a real-world cohort of patients with consistent results across spectrums of image quality and calcification.

However, our study is not without its limitations. This is an observational single center study including patients who had undergone both CCTA and SPECT with a relatively small sample size. Secondly, no comparison of ML-FFR_{CT} measurements were made with a gold standard. However, two prior studies using invasive FFR as a gold standard have shown a high degree of accuracy with no significant change in variability between operators of varying levels of expertise[20,23]. Thirdly, the studied ML prototype is not yet approved for clinical use. But a meta-analysis showing high concordance between ML- FFR_{CT} determination by machine learning (similar to our ML prototype) to invasive and computational flow dynamics, the studied ML prototype is yet not approved for clinical use[5]. Although, the two investigators who processed images had no background in CCTA interpretation, it can be argued that future application of these approaches will be carried out by non-physicians and previous studies have confirmed consistent correlation in ML-FFR_{CT} across a broad range of expertise [20].

In conclusion, we have shown a high degree of inter-operator reliability for machine learning based FFR_{CT} in a representative patient population was excellent. Our study contributes to the body of literature supporting the role of machine learning based FFR_{CT} determination in providing timely data for guiding revascularization strategies among patients being evaluated for coronary artery disease.

Declarations

Funding: Funding support for this project was provided by Siemens Medical Solutions USA.

Conflicts of interest/Competing interests: Dr Mouaz H Al-Mallah receives research support from Siemens. Drs Chris Schwemmer, Myra Cocker and Juan C Ramirez-Giraldo are employed by Siemens. No other relevant disclosures.

Code availability: Not applicable

Ethics approval and Consent to participate: Approval from the Institutional Review Board was obtained prior to the start of the study and informed consent was waived due to the retrospective nature of the study.

Consent for publication: Not applicable

Funding and Disclosures

Dr Mouaz H Al-Mallah receives research support from Siemens. Drs Chris Schwemmer, Myra Cocker and Juan C Ramirez-Giraldo are employed by Siemens. No other relevant disclosures.

References

1. Tonino PAL, De Bruyne B, Pijls NHJ, et al. Fractional flow reserve versus angiography for guiding percutaneous coronary intervention. *N Engl J Med* 2009;360:213-224.
2. Itu L, Rapaka S, Passerini T, et al. A machine-learning approach for computation of fractional flow reserve from coronary computed tomography. *J Appl Physiol (1985)* 2016;121:42-52.
3. Röther J, Moshage M, Dey D, et al. Comparison of invasively measured FFR with FFR derived from coronary CT angiography for detection of lesion-specific ischemia: Results from a PC-based prototype algorithm. *J Cardiovasc Comput Tomogr* 2018;12:101-107.
4. Coenen A, Kim Y, Kruk M, et al. Diagnostic accuracy of a machine-learning approach to coronary computed tomographic angiography-based fractional flow reserve: Result from the MACHINE consortium. *Circ Cardiovasc Imaging* 2018;11:e007217.
5. Agasthi P, Kanmanthareddy A, Khalil C, et al. Comparison of computed tomography derived fractional flow reserve to invasive fractional flow reserve in diagnosis of functional coronary stenosis: A meta-analysis. *Sci Rep* 2018;8:11535.
6. Abbara S, Blanke P, Maroules CD, et al. SCCT guidelines for the performance and acquisition of coronary computed tomographic angiography: A report of the society of cardiovascular computed tomography guidelines committee: Endorsed by the north american society for cardiovascular imaging (NASCI). *J Cardiovasc Comput Tomogr* 2016;10:435-449.
7. Cury RC, Abbara S, Achenbach S, et al. Coronary artery disease - reporting and Data System (CAD-RADS): An expert consensus document of SCCT, ACR and NASCI: Endorsed by the ACC. *JACC Cardiovasc Imaging* 2016;9:1099-1113.
8. Kueh SH, Mooney J, Ohana M, et al. Fractional flow reserve derived from coronary computed tomography angiography reclassification rate using value distal to lesion compared to lowest value. *J Cardiovasc Comput Tomogr* 2017;11:462-467.
9. Nørgaard BL, Leipsic J, Gaur S, et al. Diagnostic performance of noninvasive fractional flow reserve derived from coronary computed tomography angiography in suspected coronary artery disease: The NXT trial (analysis of coronary blood flow using CT angiography: Next steps). *J Am Coll Cardiol* 2014;63:1145-1155.
10. Koo B, Erglis A, Doh J, et al. Diagnosis of ischemia-causing coronary stenoses by noninvasive fractional flow reserve computed from coronary computed tomographic angiograms. results from the prospective multicenter DISCOVER-FLOW (diagnosis of ischemia-causing stenoses obtained

via noninvasive fractional flow reserve) study. *J Am Coll Cardiol* 2011;58:1989-1997.
11. Min JK, Leipsic J, Pencina MJ, et al. Diagnostic accuracy of fractional flow reserve from anatomic CT angiography. *JAMA* 2012;308:1237-1245.
12. Sand NPR, Veien KT, Nielsen SS, et al. Prospective comparison of FFR derived from coronary CT angiography with SPECT perfusion imaging in Stable Coronary artery disease: The ReASSESS study. *JACC Cardiovasc Imaging* 2018;11:1640-1650.
13. Hallgren KA. Computing inter-rater reliability for observational data: An overview and tutorial. *Tutor Quant Methods Psychol* 2012;8:23-34.
14. Al-Mallah MH, Ahmed AM. Controversies in the use of fractional flow reserve form computed tomography (FFR CT) vs. coronary angiography. *Current Cardiovascular Imaging Reports* 2016;9:1-7.
15. Fujimoto S, Kawasaki T, Kumamaru KK, et al. Diagnostic performance of on-site computed CT-fractional flow reserve based on fluid structure interactions: Comparison with invasive fractional flow reserve and instantaneous wave-free ratio. *Eur Heart J Cardiovasc Imaging* 2019;20:343-352.
16. Nørgaard BL, Leipsic J, Gaur S, et al. Diagnostic performance of noninvasive fractional flow reserve derived from coronary computed tomography angiography in suspected coronary artery disease: The NXT trial (analysis of coronary blood flow using CT angiography: Next steps). *J Am Coll Cardiol* 2014;63:1145-1155.
17. Lu MT, Ferencik M, Roberts RS, et al. Noninvasive FFR derived from Coronary CT angiography: Management and outcomes in the PROMISE trial. *JACC Cardiovasc Imaging* 2017;10:1350-1358.
18. Danad I, Raijmakers PG, Driessen RS, et al. Comparison of coronary CT angiography, SPECT, PET, and hybrid imaging for diagnosis of ischemic heart disease determined by fractional flow reserve. *JAMA Cardiol* 2017;2:1100-1107.
19. Gaur S, Bezerra HG, Christiansen EH, et al. Reproducibility of invasively measured and non-invasively computed fractional flow reserve. *J Am Coll Cardiol* 2014;63:A999.
20. Kumamaru KK, Angel E, Sommer KN, et al. Inter-and intraoperator variability in measurement of on-site CT-derived fractional flow reserve based on structural and fluid analysis: A comprehensive analysis. *Radiology: Cardiothoracic Imaging* 2019;1:e180012.
21. Gaur S, Bezerra HG, Lassen JF, et al. Fractional flow reserve derived from coronary CT angiography: Variation of repeated analyses. *J Cardiovasc Comput Tomogr* 2014;8:307-314.
22. Ri K, Kumamaru KK, Fujimoto S, et al. Noninvasive computed tomography-derived fractional flow reserve based on structural and fluid analysis: Reproducibility of on-site determination by unexperienced observers. *J Comput Assist Tomogr* 2018;42:256-262.
23. Ihdayhid A, Sakaguchi T, Kerrisk B, et al. Interoperator differences in diagnostic performance, precision and reproducibility of workstation-based computed tomography-derived fractional flow reserve in the detection of haemodynamically significant coronary stenosis. *Heart, Lung and Circulation* 2018;27:S248.

Figures

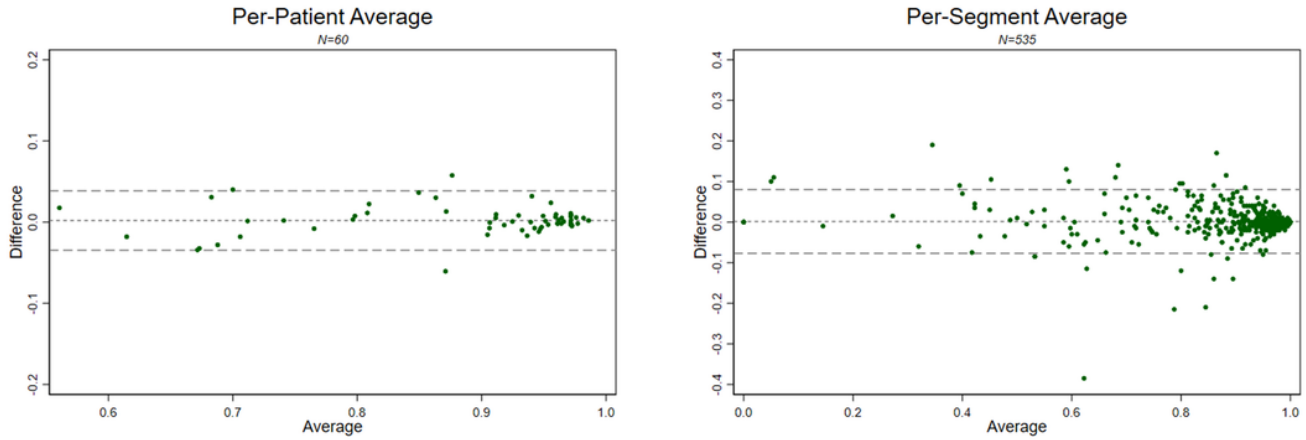

Figure 1

Bland-Altman graphs per-patient and per-segment Tight limits of agreement are seen on both per-patient and per-segment analysis

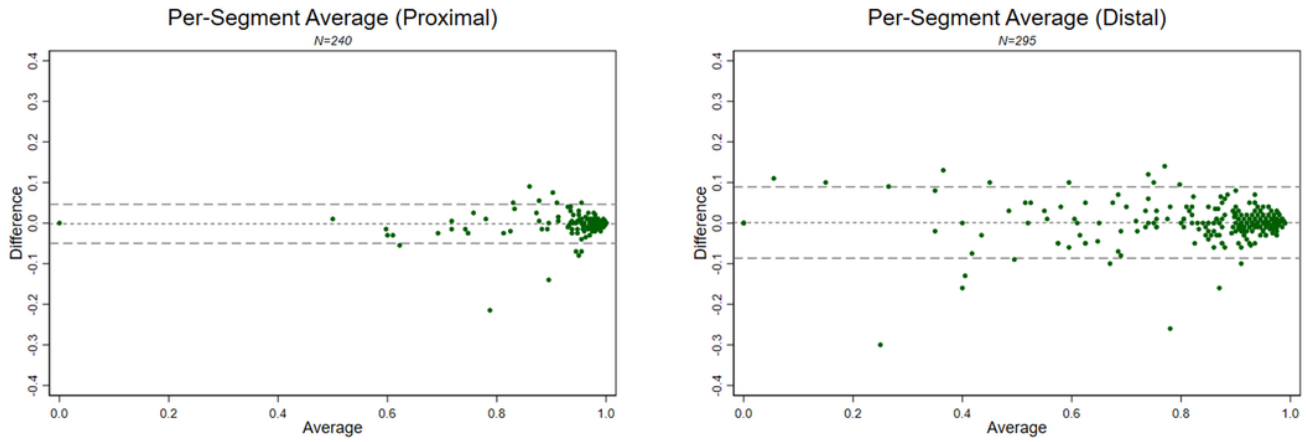

Figure 2

Bland-Altman graphs comparing proximal vs distal segments Tight limits of agreement are seen on both, with slightly wider margins in distal segments

Supplementary Files

This is a list of supplementary files associated with this preprint. Click to download.

- Supplementaltable1.docx
- SuppFig1.png